Spatiotemporal Patterns of Early Afterdepolarizations Underlying Abnormal T-Wave Morphologies in a Tissue Model of the Purkinje-Ventricular System

Mengya Yuan
Xinxiang Medical University
Pan Li (drpanli@163.com)
Xinxiang Medical University

Research Article

Keywords: Early afterdepolarization, T-wave morphology, Spatiotemporal dynamics, Cardiac modeling, Ventricular arrhythmia

Posted Date: March 17th, 2021

DOI: https://doi.org/10.21203/rs.3.rs-294397/v1

Abstract

Background

Sudden cardiac death (SCD) is a leading cause of death worldwide, and the majority of SCDs are caused by acute ventricular arrhythmias (VAs). Early afterdepolarizations (EADs) are an important trigger of VA under pathological conditions, e.g., inherited or acquired long QT syndrome (LQTS). However, it remains unclear how EAD events at the cellular level are spatially organized at the tissue level to induce and maintain ventricular arrhythmias and whether the spatial-temporal patterns of EADs at the tissue level are associated with abnormal T-wave morphologies that are often observed in LQTS, such as broad-based, notched or bifid; late appearance; and pointed T-waves.

Result

Here, a tissue model of the Purkinje-ventricular system (PVS) was developed to quantitatively investigate the complex spatial-temporal dynamics of EADs during T-wave abnormalities, and we found that (1) while major inhibition of I_{CaL} can substantially reduce the excitability of the PVS leading to conduction failures, moderate I_{CaL} inhibition can promote occurrences of AP alternans at short cycle lengths (CLs), and EAD events preferentially occur with a major reduction of I_{Kr} (> 50%) at long CLs; (2) with a minor reduction of I_{CaL}, spatially synchronized steady-state EAD events with inverted and biphasic T-waves can be “weakened” into beat-to-beat concurrences of spatially synchronized EADs and T-wave alternans, and as pacing CLs increase, beat-to-beat concurrences of localized EADs with late-appearing and pointed T-wave morphologies can be observed; (3) under certain conditions, localized EAD events in the midmyocardium may trigger slow uni-directional electric propagation with inverted (antegrade) or upright (retrograde) broad-based T-waves; (4) spatially discordant EADs were typically characterized by desynchronized spontaneous onsets of EAD events between two groups of PVS tissues with biphasic T-wave morphologies, and they can evolve into spatially discordant oscillating EAD patterns with sustained or self-terminated alternating EAD and electrocardiogram (ECG) patterns.

Conclusion

Our results provide new insights into the spatiotemporal aspects of the onset and development of EADs and suggest possible mechanistic links between the complex spatial dynamics of EADs and T-wave morphologies.

Introduction

Sudden cardiac death (SCD) is a leading cause of death worldwide, and the majority of SCDs are caused by acute ventricular arrhythmias (VA) [1, 2]. Early afterdepolarization (EAD) is the oscillation and depolarization activity of the membrane potential during action potential (AP) repolarization and

represents an important trigger for VA under pathological conditions, such as inherited or acquired long QT syndrome (LQTS)[3]. By decreasing outward currents, e.g., the rapid delayed rectifier potassium current (I_{Kr}), AP prolongation with accentuated dispersion of repolarization may give rise to EAD events originating from both Purkinje and ventricular cells in a rate-dependent manner[4], and it has been suggested that the interplay between the branching Purkinje network and ventricular tissue might play an important role in the onset and development of VA [5]. Extensive experimental or computational studies have provided mechanistic insights into the genesis of EAD at both the cellular and tissue levels [6–9]; however, it remains unclear how EAD events at the cellular level are spatially organized at the tissue level to induce and maintain ventricular arrhythmias in the Purkinje ventricular system (PVS).

Transmural dispersion of repolarization (TDR) refers to the difference in the repolarization time between midmyocardial (M) and epicardial (Epi) cells, and such a difference leads to the appearance of T-waves in electrocardiogram (ECG) recordings [10]. It was suggested that the repolarization of Epi cells corresponds to the peak of the T-wave and that of M cells corresponds to the end; therefore, the $T_{peak-end}$ (T_{pe}) interval has been proposed as the TDR index [11–14]. Although interval-based indices, e.g., QTc or T_{pe} interval, have been used in clinical practice for the risk stratification of VA, these indices neglect important information regarding spatiotemporal dispersion of repolarization present in abnormal T-wave morphologies[15], e.g., broad-based, notched or bifid, late appearance and pointed T-wave morphologies that are typically observed in LQTS patients with cardiac channelopathies in KCNQ1 (LQT1), KCNH2 (LQT2) or SCN5A (LQT3)[16]. Quantitative analysis of T-wave morphologies to evaluate flatness, notching, asymmetry and restitution properties has been proposed to provide complementary information to the QTc interval in patients with LQTS or heart failure[17–18]. However, a mechanistic link between spatial-temporal patterns of EADs at the tissue level and abnormal T wave morphologies has not been established. In this study, we developed a tissue model of the PVS to provide mechanistic insights into the onset and development of complex spatiotemporal patterns of EADs and to investigate the relationship between the spatiotemporal dynamics of EAD events and abnormal T wave morphologies.

Methods

A one-dimensional (1D) computer model of the canine PVS (~ 2 cm in length) was developed by electrically coupling mathematical models of Purkinje (P), endocardial (Endo), M and Epi cells[4, 19] via gap junctions[20] (see the model schematic in Figure S1), and an electric ratio (ER) factor was introduced to account for the asymmetrical electric properties of the Purkinje-ventricular junction (PVJ). During normal antegrade excitation, the conduction delay across the PVJ (~ 4 ms) and electric conduction velocities in each tissue type were validated according to earlier experimental measurements [21, 22]. Canine cardiac cell models (P, Endo, M and Epi) were derived from previously published Purkinje [4] and ventricular[23] cell models based on experimental measurements of intrinsic electrophysiological heterogeneities[19]. These models were developed to quantitatively represent key characteristics of intracellular Ca^{2+} cycling and membrane ionic currents specific to each cell type using similar modeling

and validation approaches[4, 23]. Extracellular unipolar potentials (as pseudo ECG signals) were computed at a site 2.0 cm away from the epicardium along the strand axis [19]. Standard programming language C was used. The forward Euler method with an adaptive time step was used for numeric integration.

To induce diverse spatiotemporal patterns of EAD, I_{Kr} and L-type calcium channels (I_{CaL}) were randomly inhibited at different levels (ranging from 0%, 10%... 100%), resulting in a total of 121 groups of dual-channel inhibition settings. With each group of settings, electric stimuli were applied at the Purkinje end of the tissue to trigger excitation at physiological pacing rates ranging from 1 Hz to 4 Hz (with a 50 ms interval in pacing cycle length (CL); 16 CLs in total), and the last two beats from each simulation were visualized as spatiotemporal maps color-coded according to the membrane potentials. The QT interval was defined as the time difference between the electric stimulation and the last cell reaching complete repolarization, and T_{pe} was defined as the time difference between the first and last cell reaching complete repolarization.

Results

Our simulation results (121 group of dual-channel inhibition settings, 16 CLs; 1936 simulations in total) can be categorized into control (16 cases), AP prolongation (864 cases), AP alternans (110 cases), EAD events (242 cases) or no excitation (704 cases). In Fig. 1, the three-dimensional (3D) parameter space defined by pacing CLs and concurrent blockade of I_{CaL} and I_{Kr} was color-coded according to excitation patterns observed in the PVS. While moderate I_{CaL} blockade ($\leq$ 60%) can promote occurrences of AP alternans at short CLs, no electric propagation and excitation can be observed with major inhibition of I_{CaL} ($\geq$ 70%); EAD events preferentially occur with major blockade of I_{Kr} ($\geq$ 50%) at long CLs. In Fig. 2A, representative subtypes of simulations were visualized as stacks of 16 two-dimensional (2D) spatiotemporal maps of membrane potential with pacing CL ranging from 250 ms to 1000 ms. In Fig. 2B, selected AP morphologies of P, Endo, M, and Epi cells (located in the center of each tissue layer) at CL = 500 ms were plotted. Under control conditions, electric stimuli trigger robust antegrade excitation under all pacing CLs with AP restitution and morphologies, depolarization and repolarization sequences, consistent with experimental findings[12]. With partial concurrent blockade (20%) of I_{Kr} and I_{CaL}, few changes in the excitation patterns can be observed, while major concurrent blockade (60%) of I_{Kr} and I_{CaL} can induce beats to beat “all or nothing” excitation patterns at pacing CL < 500 ms. With the complete inhibition of I_{Kr} and partial blockade of I_{CaL} (20%), abundant EAD events with complex spatiotemporal patterns can be observed at all pacing CLs.

Spatially synchronized EAD events

In Fig. 3A, under control conditions, electric stimuli can trigger normal antegrade excitations at CL = 750 ms with a QT interval of 247.2 ms and a T_{pe} of 20.4 ms. AP morphologies and underlying ionic currents (I_{CaL} and I_{NaL}) of selected cells (indicated as colored lines) were plotted to provide additional insights into spatiotemporal maps of excitation. At the same CLs (750 ms), a major reduction in I_{Kr} (80%) induced

substantial AP prolongation and spatially synchronized EAD events with inverted and biphasic T-waves (QT = 566.4 ms; T_{pe}=44.4 ms) (Fig. 3B). During spatially synchronized EAD events, all types of tissues simultaneously developed EAD upstrokes at -22 mV, with different EAD amplitudes (31.18 mV in Epi cells; 15.11 mV in P cells), and while I_{CaL} was reactivated to induce EAD in the myocardium tissues, it was mostly I_{NaL} in Purkinje cells[4]. When combined with a minor reduction in I_{CaL} (20%), the effects of an 80% reduction in I_{Kr} were "weakened" to induce beat-to-beat occurrences of synchronized EADs and T-wave alternans (QT = 323.2 ms, 596.2 ms; T_{pe}=36.0 ms, 32.8 ms) (Fig. 3C).

Localized EAD events

Interestingly, as pacing CLs increase (from 750 ms to 850 ms; Fig. 4A), localized EAD events may exclusively arise from midmyocardial tissues to significantly prolong QT (443.2 ms; ↑37%) and T_{pe} (82.4 ms; ↑129%) intervals, with late-appearing (QT prolongation) and pointed (exclusive EADs in the midmyocardium) T-wave morphology[24] and T-wave alternans with reduced beat-to-beat variations in QT intervals (QT = 443.2 ms, 596.9 ms; ↓47%) and increased beat-to-beat differences in T_{pe} (T_{pe}=82.4 ms, 33.6 ms; ↑1425%). In Fig. 4B, under certain conditions (complete inhibition of I_{Kr} and 20% reduction of I_{CaL} at CL = 550 ms), localized EAD events can synchronously arise from two neighboring tissue types, i.e., M and Epi tissues and led to inverted, asymmetric broad-based T-wave morphology[25] in the first beat (QT = 504.8 ms; T_{pe}=172.8 ms) and T-wave alternans with substantial beat-to-beat variations in T_{pe} intervals (T_{pe}=172.8 ms, 43.2 ms).

Localized-EAD-induced unidirectional propagation

In Fig. 5, localized EAD events can act as a focal source of arrhythmogenic and trigger spontaneous antegrade or retrograde excitations in the PVS. With a 70% reduction in I_{Kr} at CL = 500 ms, EAD can spontaneously arise from the midmyocardium and trigger unidirectional electric propagation towards the epicardium with a time delay in the onset of EAD and reactivation of I_{CaL} between the M and Epi cells (Fig. 5A), leading to an inverted and notched T-wave (QT = 503.6 ms; T_{pe}=162.9 ms). In Fig. 5(B)(C), with 60% reduction of I_{Kr}, spontaneous EAD in the midmyocardium (beat #2) can trigger retrograde excitation in the PVS at CL = 650 ms with a conduction velocity (CV) of 0.2 m/s, and sequential development of EAD upstrokes from M cells to Endo and P cells (Fig. 5B) with a broad-based asymmetric T-wave (QT = 488.3 ms; T_{pe}=172.4 ms); at a slower pacing rate (CL = 850 ms), a much slower spontaneous retrograde conduction (CV = 0.1 m/s) can be observed (beat #1) with an increase in both QT interval (514.4 ms) and T_{pe}(192.0 ms) and a broad-based T-wave.

Spatially desynchronized EAD events and oscillatory excitation patterns

In addition to spatially synchronized EAD events, as seen in Fig. 3(B)(C), spatially discordant development of EADs can also be induced under certain conditions, typically with a biphasic T-wave morphology. In Fig. 6(A), with 60% I_{Kr} inhibition at CL = 900 ms, partially synchronized EAD development

in P, Endo and M cells (beat #1) preceded the beat-to-beat spontaneous onset of EAD in the epicardium by 90 ms, with no EAD-induced electric propagation from M to Epi cells, as seen in Fig. 5(A). These spatiotemporal excitation patterns give rise to interesting spatial T-wave alternans with alternating biphasic (QT = 594.4 ms; TDR = 83.2 ms; with notching) and monophasic (QT = 489.6 ms; TDR = 168.0 ms; broad-based) T-wave morphologies. With 70% I_{Kr} inhibition at CL = 750 ms (Fig. 6B), focal EAD arising from the midmyocardium triggered bidirectional excitations towards both the epi- and endocardium with a late-appearing spontaneous onset of EADs in the P cells, leading to a biphasic T-wave without notching.

In Fig. 6(C), complete inhibition of I_{Kr} (CL = 600 ms) can induce severe and complex spatiotemporal patterns of EADs in all tissue types. The first electric stimulus successfully triggered antegrade propagation of excitation with spatially synchronized EADs in the Endo-, M- and epicardium; after the application of the second electric stimulus, spatially discordant development of oscillating EAD waveforms with alternating EAD occurrences in the M- and epicardium or in the Purkinje tissue and endocardium was observed, leading to focal reentrant behaviors and a sustained oscillatory ECG pattern typically observed during ventricular tachycardia[26]. In Fig. 6(D), with a complete blockade of I_{Kr} and a 10% reduction in I_{CaL} (CL = 400 ms), localized EAD events in the epicardium during previous repolarization may collide with the current wavefront of depolarization and trigger self-terminated oscillatory EAD patterns. Two electric stimuli (CL = 400 ms) were applied during the simulation, and while two complete APs could be observed in the Purkinje tissue (stimulus-to-response ratio of 2:2), there was only one single AP with oscillatory EADs in the epicardium (stimulus-to-response ratio of 2:1).

Discussion

In this paper, we presented a 1D tissue model of the PVS and investigated a wide range of complex spatiotemporal patterns of EAD events by exploring the three-dimensional parameter space defined by I_{Kr}, I_{CaL} and pacing CLs. Our results suggested that while major inhibition of I_{CaL} (> 60%) can substantially reduce the excitability of the PVS and cause conduction failures, moderate I_{CaL} inhibition can promote occurrences of AP alternans at short CLs; EAD events preferentially occur with a major reduction in I_{Kr} (≥ 50%) at long CLs. With a minor reduction in I_{CaL}, spatially synchronized steady-state EAD events with inverted and biphasic T-waves can be “weakened” into beat-to-beat concurrences of spatially synchronized EADs and T-wave alternans and beat-to-beat concurrences of localized EADs (e.g., in the midmyocardium) with late-appearing and pointed T-wave morphologies as pacing CLs increase. Under certain conditions, these localized EAD events in the midmyocardium can act as a focal source of arrhythmogenicity and trigger slow unidirectional electric propagation with inverted (antegrade) or upright (retrograde) broad-based T-waves. In contrast to localized EAD-triggered electric propagation, spatially discordant EADs are typically characterized by desynchronized spontaneous onset of EAD events between different groups of tissues with biphasic T-wave morphologies, and they can evolve into spatially discordant oscillating EAD patterns with sustained or self-terminated alternating EAD and ECG patterns.

These findings provide new insights into the spatiotemporal aspects of the onset and development of EADs and suggest possible mechanistic links between the complex spatial dynamics of EADs and T-wave morphologies. T-waves, or ECG signals in general, are high-level abstractions of the electric behaviors of a 3D complex biological system (i.e., the mammalian heart), and there can be diverse multiscale mechanisms underlying common T-wave morphologies[27]. Although limited by the 1D nature of our PVS model, our findings could be useful in advancing our understanding of the spatiotemporal aspects of T-wave abnormalities. Further development of human-specific systems models of PVS[28] is required to simulate complex interactions between the human Purkinje network and ventricular systems and to provide computational tools to accelerate the prevention and treatment of lethal ventricular arrhythmias.

Declarations

Ethics approval and consent to participate

Not applicable.

Consent for publication

Not applicable.

Availability of data and materials

Not applicable.

Competing interests

None.

Funding

This study was supported by the National Science Foundation of China (Grant No. U1904158 and U1604178) to P.L.

Authors' contributions

P.L. designed the study. M.Y. performed the computer simulation and prepared all figures. P.L. and M.Y. analyzed the results, and wrote the manuscript together.

Acknowledgement

None.

References

1. Kuriachan, V. P., Sumner, G. L., & Mitchell, L. B. (2015). Sudden cardiac death. Current problems in cardiology, 40(4), 133–200. doi.org/10.1016/j.cpcardiol.2015.01.002
2. Hayashi, M., Shimizu, W., & Albert, C. M. (2015). The spectrum of epidemiology underlying sudden cardiac death. Circulation research, 116(12), 1887–1906. doi.org/10.1161/CIRCRESAHA.116.304521
3. Shimizu, W., Ohe, T., Kurita, T., Takaki, H., Aihara, N., Kamakura, S., Matsuhisa, M., & Shimomura, K. (1991). Early afterdepolarizations induced by isoproterenol in patients with congenital long QT syndrome. Circulation, 84(5), 1915–1923.
4. Li, P., & Rudy, Y. (2011). A model of canine purkinje cell electrophysiology and Ca^{2+} cycling: rate dependence, triggered activity, and comparison to ventricular myocytes. Circulation research, 109(1), 71–79. https://doi.org/10.1161/CIRCRESAHA.111.246512
5. Haissaguerre, M., Vigmond, E., Stuyvers, B., Hocini, M., & Bernus, O. (2016). Ventricular arrhythmias and the His-Purkinje system. Nature reviews. Cardiology, 13(3), 155–166. https://doi.org/10.1038/nrcardio.2015.193
6. Tran, D. X., Sato, D., Yochelis, A., Weiss, J. N., Garfinkel, A., & Qu, Z. (2009). Bifurcation and chaos in a model of cardiac early afterdepolarizations. Physical review letters, 102(25), 258103. https://doi.org/10.1103/PhysRevLett.102.258103
7. Huang, X., Song, Z., & Qu, Z. (2018). Determinants of early afterdepolarization properties in ventricular myocyte models. PLoS computational biology, 14(11), e1006382. doi.org/10.1371/journal.pcbi.1006382
8. Vandersickel, N., Van Nieuwenhuyse, E., Seemann, G., & Panfilov, A. V. (2017). Spatial Patterns of Excitation at Tissue and Whole Organ Level Due to Early Afterdepolarizations. Frontiers in physiology, 8, 404. https://doi.org/10.3389/fphys.2017.00404
9. Tazmini, K., Frisk, M., Lewalle, A., Laasmaa, M., Morotti, S., Lipsett, D. B., Manfra, O., Skogestad, J., Aronsen, J. M., Sejersted, O. M., Sjaastad, I., Edwards, A. G., Grandi, E., Niederer, S. A., Øie, E., & Louch, W. E. (2020). Hypokalemia Promotes Arrhythmia by Distinct Mechanisms in Atrial and Ventricular Myocytes. Circulation research, 126(7), 889–906. https://doi.org/10.1161/CIRCRESAHA.119.315641
10. Antzelevitch C (2005) Role of transmural dispersion of repolarization in the genesis of drug-induced torsades de pointes. Heart rhythm 2: S9-155.
11. Antzelevitch C (2001) Transmural dispersion of repolarization and the T wave. Cardiovascular research 50: 426–431.
12. Yan GX, Antzelevitch C (1998) Cellular basis for the normal T wave and the electrocardiographic manifestations of the long-QT syndrome. Circulation 98 (18): 1928–1936.
13. Antzelevitch C (1997) The M Cell. Journal of cardiovascular pharmacology and therapeutics 2 (1): 73–76.
14. Lubinski A 1, Lewicka-Nowak E, Kempa M, Baczynska AM, Romanowska I, Swiatecka G. (1998) New insight into repolarization abnormalities in patients with congenital long QT syndrome: the increased transmural dispersion of repolarization. Pacing Clin Electrophysiol 21: 172–175.

15. Ramírez, J., Orini, M., Mincholé, A., Monasterio, V., Cygankiewicz, I., Bayés de Luna, A., Martínez, J. P., Pueyo, E., & Laguna, P. (2017). T-Wave Morphology Restitution Predicts Sudden Cardiac Death in Patients With Chronic Heart Failure. Journal of the American Heart Association, 6(5), e005310. https://doi.org/10.1161/JAHA.116.005310
16. Wallace, E., Howard, L., Liu, M., O'Brien, T., Ward, D., Shen, S., & Prendiville, T. (2019). Long QT Syndrome: Genetics and Future Perspective. Pediatric cardiology, 40(7), 1419–1430. https://doi.org/1007/s00246-019-02151-x
17. Porta-Sánchez, A., Spillane, D. R., Harris, L., Xue, J., Dorsey, P., Care, M., Chauhan, V., Gollob, M. H., & Spears, D. A. (2017). T-Wave Morphology Analysis in Congenital Long QT Syndrome Discriminates Patients From Healthy Individuals. JACC. Clinical electrophysiology, 3(4), 374–381. https://doi.org/10.1016/j.jacep.2016.10.013
18. Ramírez, J., Orini, M., Mincholé, A., Monasterio, V., Cygankiewicz, I., Bayés de Luna, A., Martínez, J. P., Pueyo, E., & Laguna, P. (2017). T-Wave Morphology Restitution Predicts Sudden Cardiac Death in Patients With Chronic Heart Failure. Journal of the American Heart Association, 6(5), e005310. https://doi.org/10.1161/JAHA.116.005310
19. Zhao, Ping'an & Li, Pan. (2019). Transmural and rate-dependent profiling of drug-induced arrhythmogenic risks through in silico simulations of multichannel pharmacology. Scientific Reports. 9(1): 18504. Doi:10.1038/s41598-019-55032-x.
20. Gima, K., & Rudy, Y. (2002). Ionic current basis of electrocardiographic waveforms: a model study. Circulation research, 90(8), 889–896. https://doi.org/10.1161/01.res.0000016960.61087.86
21. Veenstra, R. D., Joyner, R. W., & Rawling, D. A. (1984). Purkinje and ventricular activation sequences of canine papillary muscle. Effects of quinidine and calcium on the Purkinje-ventricular conduction delay. Circulation research, 54(5), 500–515. https://doi.org/10.1161/01.res.54.5.500
22. Wiedmann, R. T., Tan, R. C., & Joyner, R. W. (1996). Discontinuous conduction at Purkinje-ventricular muscle junction. The American journal of physiology, 271(4 Pt 2), H1507–H1516. https://doi.org/10.1152/ajpheart.1996.271.4.H1507
23. Decker, K. F., Heijman, J., Silva, J. R., Hund, T. J., & Rudy, Y. (2009). Properties and ionic mechanisms of action potential adaptation, restitution, and accommodation in canine epicardium. American journal of physiology. Heart and circulatory physiology, 296(4), H1017–H1026. https://doi.org/10.1152/ajpheart.01216.2008
24. Orhan U. Kilinc, Volkan Tuzcu (2011) Successful Elimination of Significant Arrhythmia Burden with Flecainide in an Adolescent with Long QT Syndrome Type 3. Congenital heart disease 7 (4): E42-5.
25. Skinner J, Morrow P (2015) Cardiac genetic investigation of sudden cardiac death: advances and remaining limitations. Research and Reports in Forensic Medical Science 5: 7–15.
26. Gan-Xin Yan, Ying Wu, Tengxian Liu, Jixin Wang, Roger A. Marinchak, Peter R. Kowey (2001) Phase 2 Early Afterdepolarization as a Trigger of Polymorphic Ventricular Tachycardia in Acquired Long-QT Syndrome. Circulation 103: 2851–2856.

27. Sieira, J., Dendramis, G., & Brugada, P. (2016). Pathogenesis and management of Brugada syndrome. Nature reviews. Cardiology, 13(12), 744–756. https://doi.org/10.1038/nrcardio.2016.143

28. Trovato, C., Passini, E., Nagy, N., Varró, A., Abi-Gerges, N., Severi, S., & Rodriguez, B. (2020). Human Purkinje in silico model enables mechanistic investigations into automaticity and pro-arrhythmic abnormalities. Journal of molecular and cellular cardiology, 142, 24–38. https://doi.org/10.1016/j.yjmcc.2020.04.001

Figures

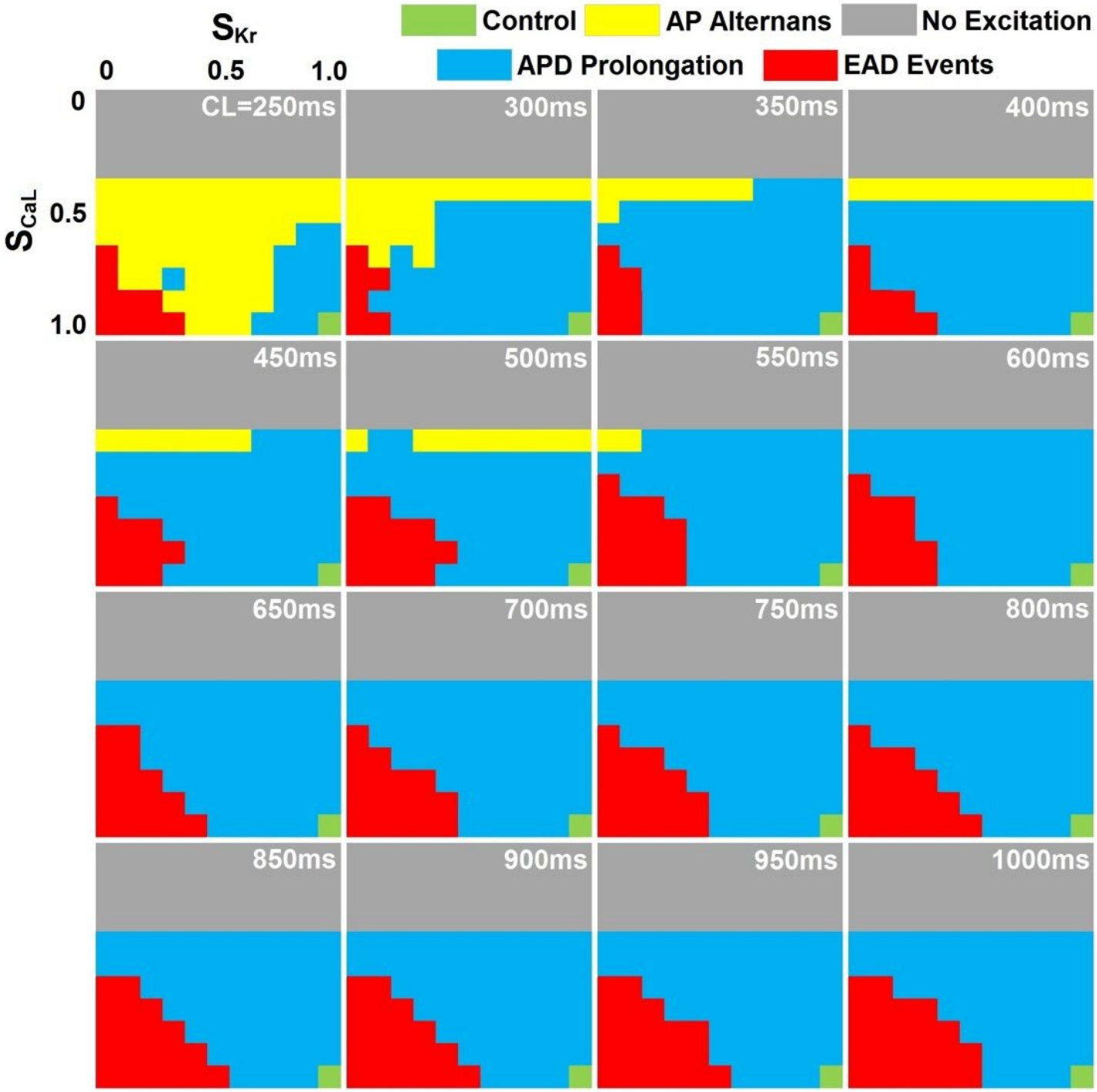

Figure 1

Parameter space mapping of SKr, SCaL and CL, color-coded according to spatiotemporal excitation patterns of the PVS (control: green; gray: no excitation; blue: action potential (AP) prolongation; yellow: AP alternans without early afterdepolarization (EAD) events; red: EAD events). SKr: the scaling factor of IKr inhibition; SCaL: the scaling factor of ICaL inhibition; CL: pacing cycle length.

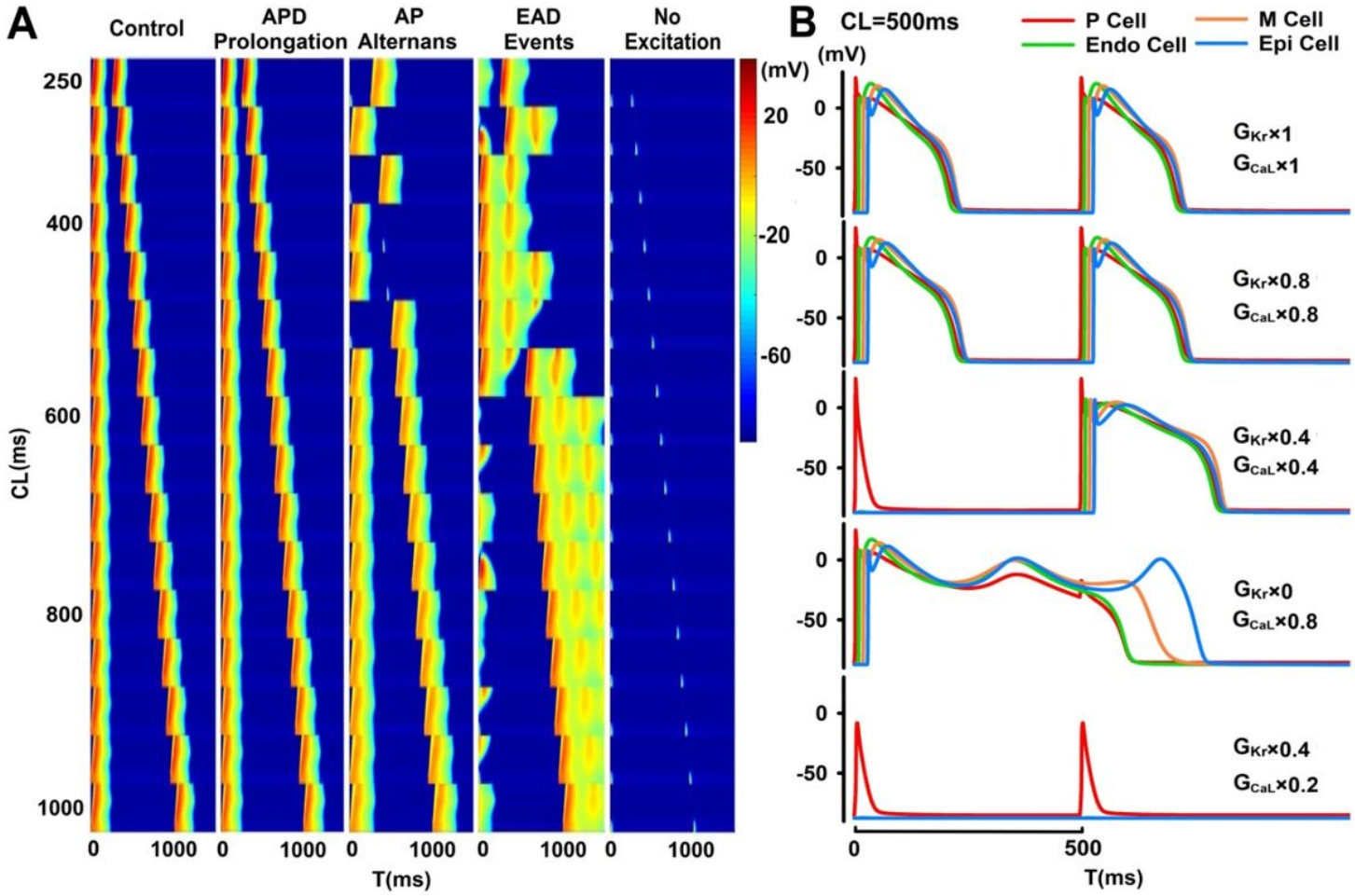

Figure 2

(A) Representative groups of simulations of the PVS tissue model with minor changes, AP alternans, EAD events or no excitation, where the group of simulations were visualized as a stack of 16 spatiotemporal maps with pacing CLs ranging from 250 ms (top) to 1000 ms (bottom). (B) Representative AP morphologies of each cell type at CL=500 ms under control (top) and pathological conditions.

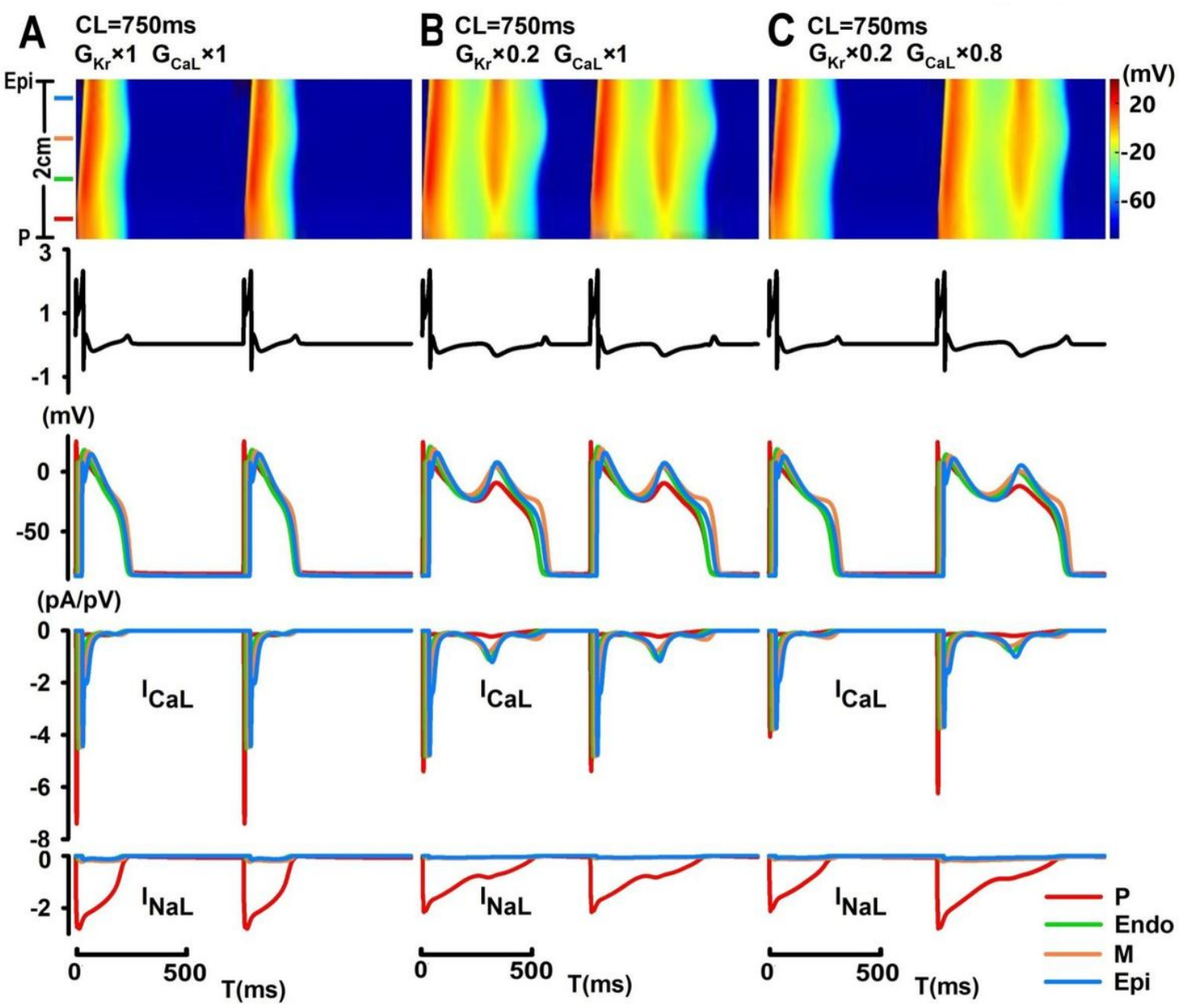

Figure 3

Computer simulation of spatially synchronized EAD events in the PVS tissue model. (A) Normal antegrade excitation of the PVS under control conditions; (B) spatially synchronized steady-state EAD events with T-wave inversion can be induced by an 80% reduction in IKr at CL=750 ms and degraded into beat-to-beat occurrences of spatially synchronized EADs and T-wave alternans with an additional blockade of ICaL (20%) (C).

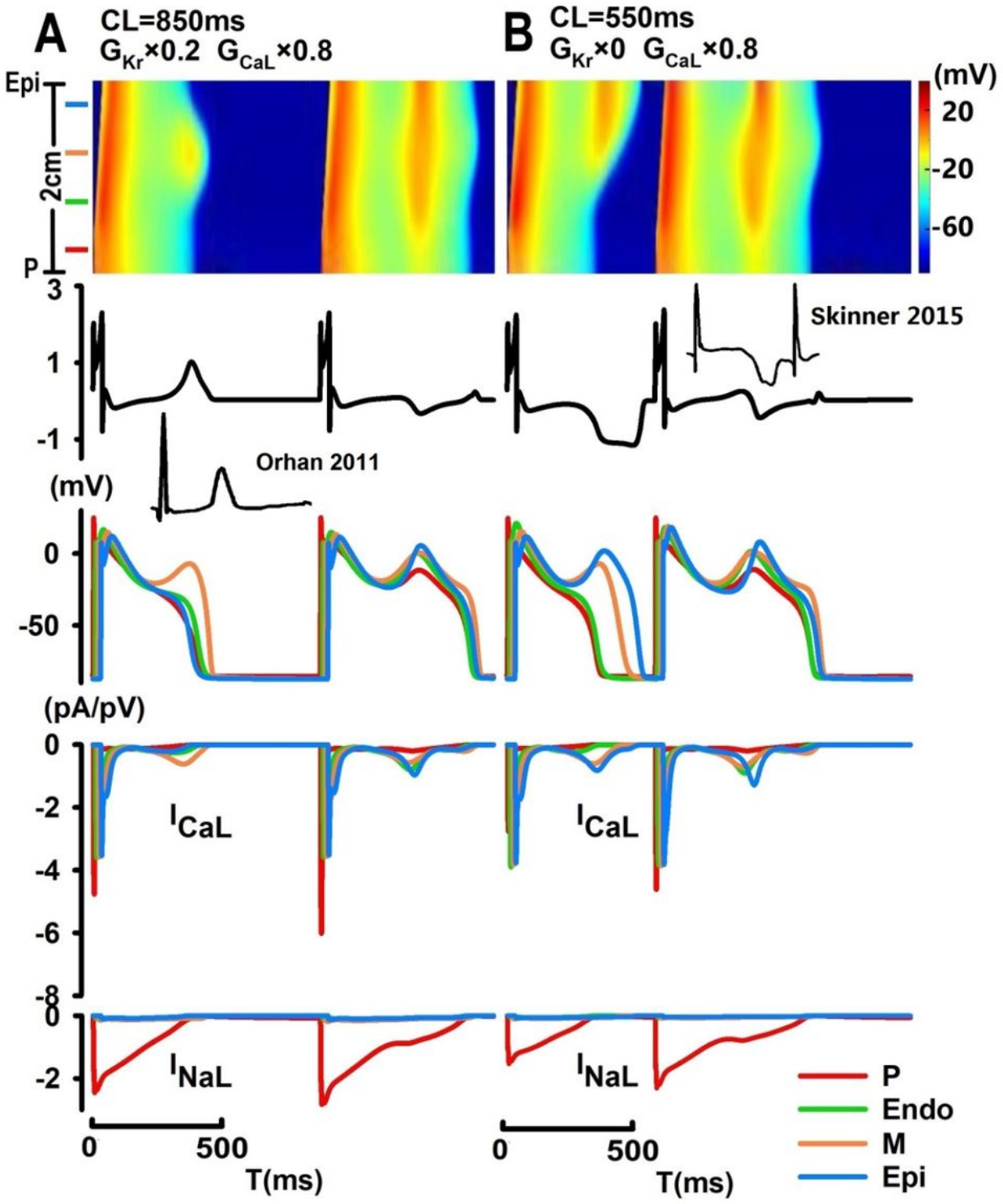

Figure 4

Computer simulation of localized EAD events. (A) With an 80% reduction in IKr and a 20% reduction in ICaL, localized EAD can arise exclusively from the midmyocardium at CL=850 ms, with a late-appearing and pointed T-wave; (B) with complete inhibition of IKr and a 20% reduction in ICaL, localized EAD can arise simultaneously in the mid- and epicardium, with an inverted broad-based T-wave.

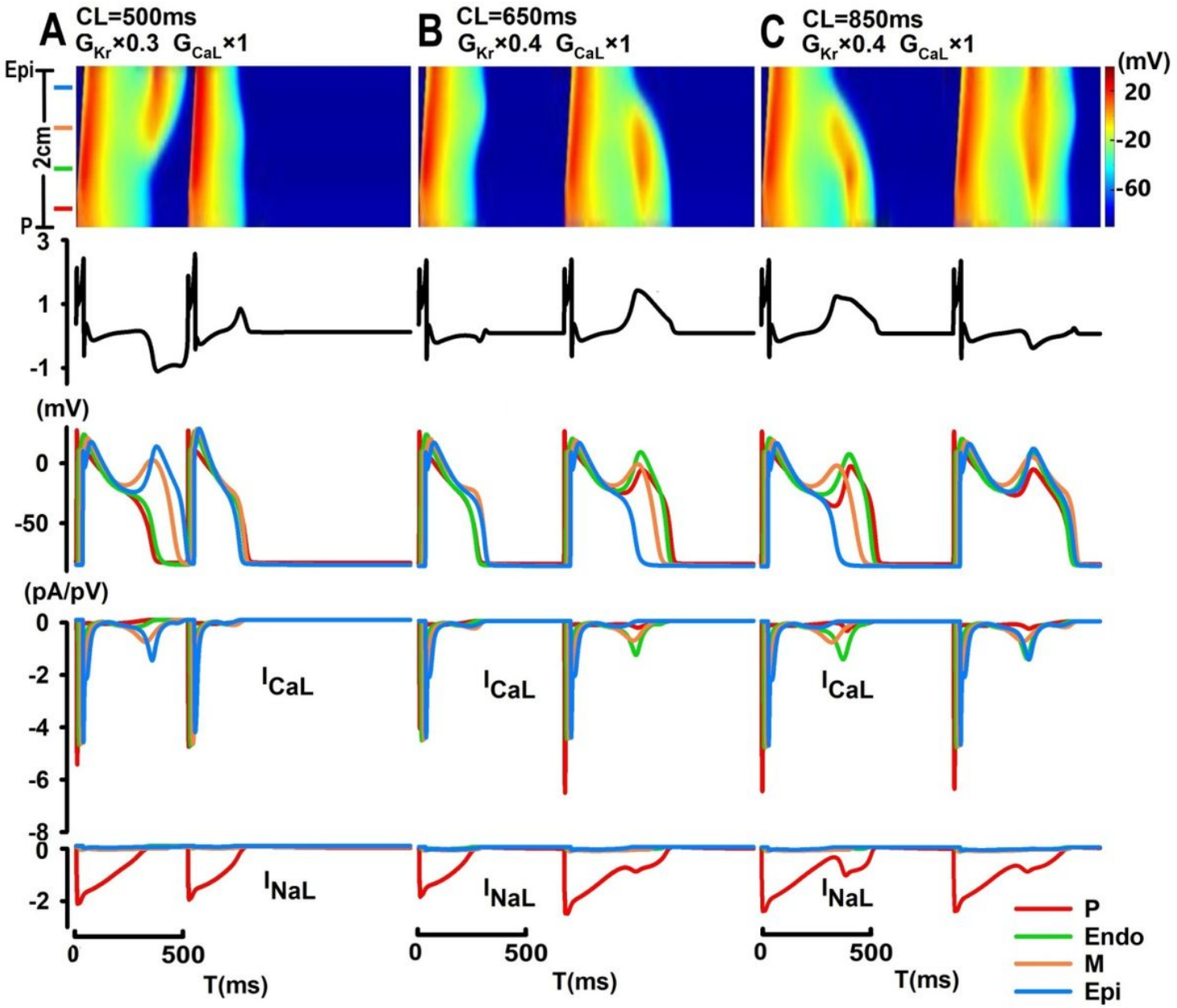

Figure 5

Computer simulation of EAD-induced unidirectional electric propagation. Localized EAD arising from the midmyocardium can trigger spontaneous antegrade propagation with a 70% blockade of IKr (CL=500 ms) (A) and spontaneous retrograde propagation with a 60% blockade of IKr at CL=650 ms (conduction velocity (CV)=0.2 m/s; (B)) and at CL=850 ms (CV=0.1 m/s; (C)).

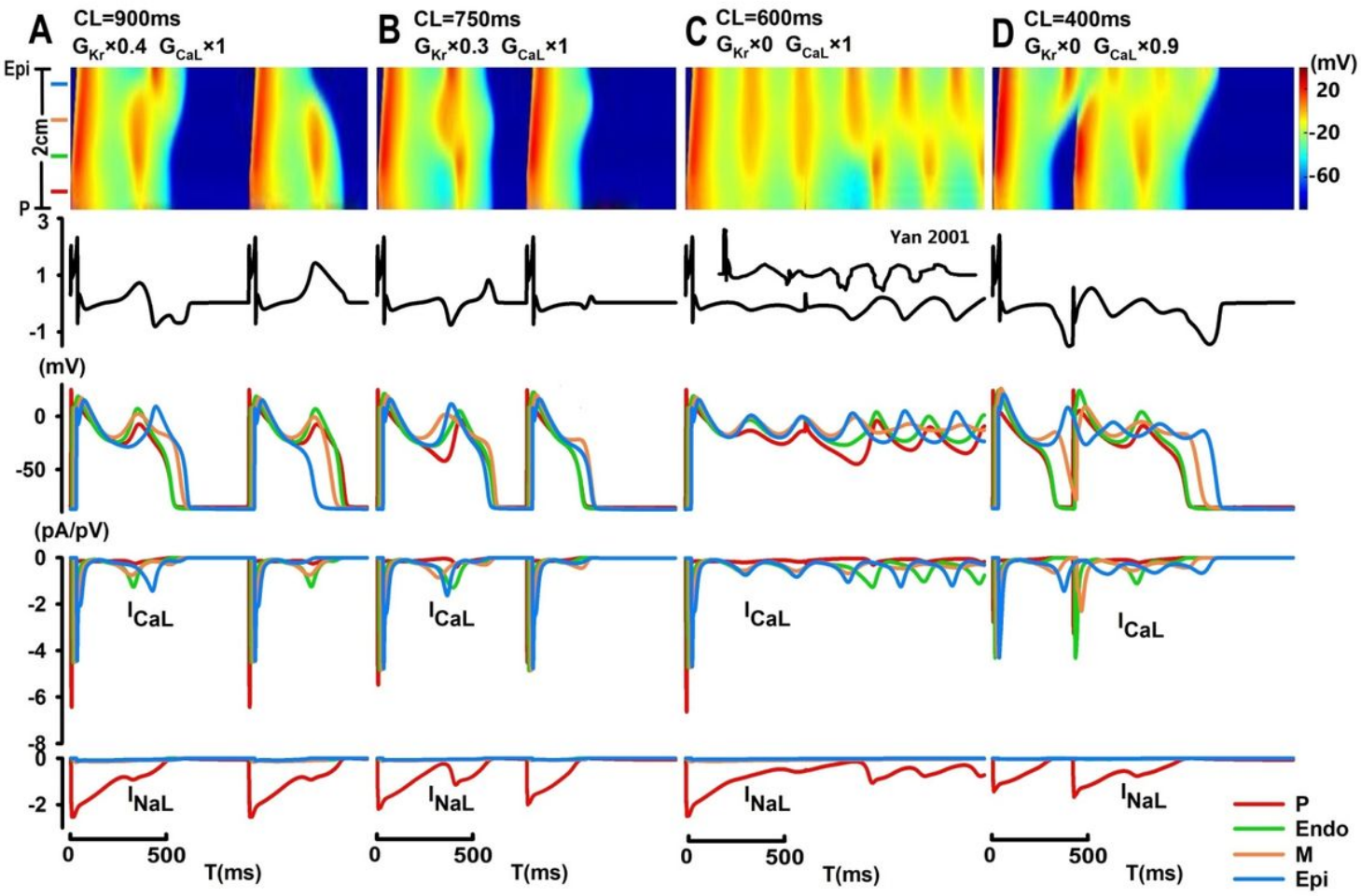

Figure 6

Computer simulation of spatially desynchronized EAD events and oscillatory excitation patterns. (A) Partially synchronized EAD development in P, Endo and M cells preceded the beat-to-beat spontaneous onset of EAD in the epicardium; (B) focal EAD arising from the midmyocardium triggered bidirectional excitation with a late-appearing spontaneous onset of EADs in the P tissue; (C) spatially discordant development of oscillating EAD and ECG patterns with sustained alternating EAD occurrences in the M- and epicardium or in the Purkinje tissue and endocardium; (D) localized EAD events in the epicardium during previous repolarization collided with the current wavefront of depolarization and triggered self-terminated oscillatory EAD and ECG patterns.

Supplementary Files

This is a list of supplementary files associated with this preprint. Click to download.

- EADsupplement.docx